Astronomy VLBA campaign MOJAVE used in geodesy

Hana Krásná · Leonid Petrov

Abstract Insert your abstract here.

1 Introduction

MOJAVE (Monitoring Of Jets in Active galactic nuclei with VLBA (Very Long Baseline Array) Experiments) is a long-term program carried out by an astrophysics community, which focuses on monitoring of radio brightness and polarization variations in jets associated with active galaxies on parsec-scales visible in the northern sky (Lister et al., 2018). In September 2016 the observing series with the VLBA observation code "BL229" has started. In this series, the observations are carried out at a wavelength of 2 cm (15 GHz, Ku-band) approximately every month within 2048 Mbps 24 hour-long experiments. In this publication, we show for the first time the capability of astrophysics VLBA measurements to provide estimates of the geodetic parameters, such as Earth orientation parameters or terrestrial reference frame on a comparable accuracy level as the dedicated geodetic VLBA sessions. The Earth orientation parameters, which built the link between the terrestrial and celestial reference frame, are regularly estimated by Very Long Baseline Interferometry.

H. Krásná
1. TU Wien, Department of Geodesy and Geoinformation, Wien, Austria
2. Astronomical Institute of the Czech Academy of Sciences, Prague, Czech Republic
E-mail: hana.krasna@tuwien.ac.at

L. Petrov
NASA Goddard Space Flight Center, Code 61A, Greenbelt, USA

The unsubstitutable role of VLBI is in the measurement of UT1-UTC and nutation components. Until recently, the estimates of EOP were produced only from the observations in the traditional S/X bands (2.3/8.6 GHz, 13/3.6 cm). In Krásná et al. (2019) the first estimates of the EOP from the dedicated geodetic VLBA experiments in K-band (24 GHz, 1.2 cm) were published. In this paper, we present the first EOP estimates in Ku-band (15 GHz, 2 cm) from purely astrophysics VLBA sessions covering the last four years (2016.7 — 2020.5). In Krásná and Petrov (2021, in preparation) we further focus on the MOJAVE data from the astrometry point of view, dealing with the estimated radio source positions which built a celestial reference frame.

2 Data analysis

The VLBA network consists of ten 25-meters radio telescopes located on U.S. territory (eight in North America, one in the Pacific, and one in the Caribbean), see Fig. 1. The dataset "BL229" from the VLBA correlator is publicly available through the National Radio Astronomy Observatory (NRAO) Science Data archive[1] in the FITS-IDI (Interferometry Data Interchange) format. This observing series started on September 26, 2016 and we include the first 33 experiments with the last one on July 02, 2020 in this publication. In the first 25 experiments (BL229aa-ay) the observed Ku-band is split into eight sub-bands with an individual bandwidth of 32 MHz including 64 channels each. Since July 2019 (experiment BL229az) the bandwidth of a sub-band has increased to 64 MHz, which built four sub-bands covering 128 channels (see Table 1). We processed the observations with the fringe-fitting software PIMA (Petrov
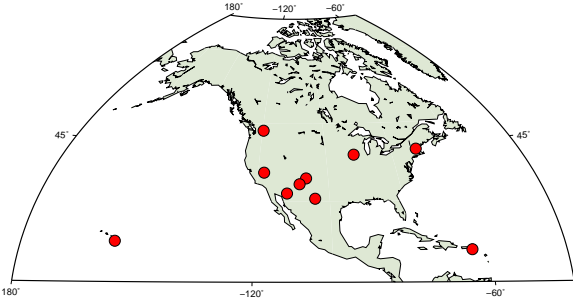
---

[1] https://archive.nrao.edu/archive

Fig. 1 Distribution of the ten VLBA radio telescopes.

Table 1 Lower edge frequency of the sub-bands in the BL229 experiments in GHz.

BL229aa-ay	BL229az-bg
15.22400	15.17575
15.25600	15.25575
15.28800	15.31975
15.32000	15.38375
15.35200	
15.38400	
15.41600	
15.44800	

et al., 2011) (coarse fringe fitting – bandpass calibration – fine fringe fitting) and produced databases including among others group delays and their uncertainties in a geo-VLBI format GVH and its plain ascii database counter-part VGOSDA, or for short VDA[2]. These databases serve as input for the data analysis software package pSolve[3] and as an alternative input for the analysis software package VieVS (Böhm et al., 2018).
(DO WE WANT TO GIVE MORE DETAILS FOR THE FRINGE FITTING, OR FLAGGING OF OUTLIERS?)

We process the MOJAVE group delays with these two independent analysis software packages and compare the estimated baseline lengths and Earth orientation parameters in terms of the weighted root mean square. Furthermore, we analyse the geodetic RDV and CN sessions observed in S/X band for the same time span (starting with RV119 on September 14, 2016 until RV141 on July 07, 2020) which are 22 RDV and 6 CN experiments in total. RDV sessions are astrometric/geodetic sessions scheduled for full ten stations VLBA network plus up to ten geodetic stations capable of recording VLBA modes. These sessions are scheduled to provide among others accurate EOP and a high

accuracy TRF where the VLBA stations are incorporated into the VLBI reference frame through the inclusion of other geodetic stations with long history of observations. The CN experiments consist of the ten VLBA stations only and run concurrent with the Rapid turnaround Monday IVS sessions (IVS-R1). We show the comparison of the baseline length scatter between the VLBA telescopes and of the estimated EOP from the astrophysics VLBA measurements and from the dedicated geodetic experiments.

Besides the comparison of the estimated geodetic parameters from two diverse VLBA datasets, we take the opportunity to show the differences in the estimated parameters due to the use of different software packages. Therefore, we analyse the VLBA data in several ways. The first solution was produced using the software PIMA for the fringe-fitting and pSolve for the analysis. In the second solution we analysed the group delays produced with the PIMA software with the analysis software VieVS. For the RDV&CN experiments we run a third solution where we use the official vgosDB database maintained by the IVS Data Centers and analysed it with the software VieVS.

Table 2 summarizes the a priori models used in pSolve and VieVS during the group delay analysis. Tables 3 and 4 contain the parametrization of the estimated parameters in the solutions. The MOJAVE and RDV&CN experiments are processed in the same manner with the same parametrization to allow for an informative comparison. But there are several important differences between the datasets. One of them is the fact, that MOJAVE sessions are single-band experiments. This causes the impossibility to correct the measurements for the ionospheric delay by using the observations in two radio bands as it is done for the RDV&CN experiments. We concentrate on this issue in detail in Section 3. Another difference is the scheduling approach due to the different goals of the experiments. In Fig. 2 we show the sky coverage during a 24-hour observing session at three selected telescopes (BR-VLBA, FD-VLBA, SC-VLBA) where colors depict the time passed since the start of the session. As an example we show the sky coverage during the MOJAVE session BL229bc observed on December 22, 2019 in the upper plots and the CN1924 session observed with the same network on December 09, 2019 in the lower plots. Table 5 summarizes the mean number of scans in a 24-hour experiment at each of the ten VLBA telescopes computed over the investigated time period (September 2016 - July 2020). The numbers show, that during geodetic experiments there are twice as many scans at each telescope as during the MOJAVE sessions. The geodetic sessions focus on even distribution of the observations over all azimuth

---

Table 2 A priori models used in the analysis

	pSolve	VieVS
CRF	gsf_2020c	ICRF3 (Charlot et al., 2020) including Galactic Aberration
TRF	gsf_2020c	ITRF2014 (Altamimi et al., 2016)
precession/nutation model	IAU2006/2000A	(Mathews et al., 2002; Capitaine et al., 2003)
EOP	gsf_2020c (heo_20200606.heo)	14C04
non-tidal atmosphere loading	merra2_geosfpit	Vienna APL

Table 3 Parametrization of estimated parameters of the single session solutions in pSolve

	pSolve
CRF	selected sources with constraint sigma 20 as
TRF	NNT/NNR condition on VLBA stations with 0.1 mm constraints
polar motion	offset and rate with constraint sigma 45 mas on offset
UT1	offset and rate with constraint sigma 3 ms on offset
celestial pole offsets	offset without constraints
zenith wet delay	B-spline with the time span 20 min and sigma of constraints 50.00 ps/h
tropo. gradients	8 hours with sigma of constr. 0.5 mm on offset and 2.00 mm/day on rate
clocks	B-spline with the time span 60 min and constraint sigma 5.e-14 s/s
baseline clock offsets	offset with constraint sigma 500 ns
weights	yes

Table 4 Parametrization of estimated parameters of the single session solutions in VieVS

	VieVS
CRF	selected sources without contraints
TRF	NNT/NNR condition on VLBA stations
polar motion	pwlo with the time span 24 hours with relative constraints 1 mas
EOP	offset
zenith wet delay	pwlo with time span 30 min with relative constraints 1.5 cm
tropo. gradients	pwlo with time span 180 min with relative constraints 0.5 cm
clocks	pwlo with time span 60 min with relative constraints 1.3 cm, one rate and one quadratic term per clock
baseline clock offsets	offset without constraints
weights	baseline-dependent weighting

and elevation angles in the common visibility sky area to ensure a good decorrelation of station dependent parameters such as station height, zenith wet delay, clock parameters or baseline clock offsets. On the other hand, the primary goal of the BL229 experiments is in monitoring of jets in active galactic nuclei, therefore the schedule is optimized to track a set of sources in a 24-hour session. The Fig. 3 depicts the total number of observed sources in each session (upper plot) and the median number of observations during a 24-hour session for each source computed over the respective four years period. The red crosses show the MOJAVE sessions, and blue x-signs depict the RDV&CN sessions. The median of observed sources lies at 30 radio sources during a MOJAVE session, and at 78 radio sources during a RDV&CN session. Comparison of the number of observations for each source during a whole session shows that 95% of the AGN observed in MOJAVE sessions have more than 150 observations whereas only 35% of the sources observed in RDV&CN sessions gets over

this limit. This shows again the interest of MOJAVE sessions to obtain enough data for particular sources during an experiment to allow for imaging and astrophysics study. Sources with few observations in geodetic experiments served for a good sky coverage over the stations which allows an accurate estimation of geodetic relevant parameters.

Baseline length repeatability. We run several solutions which we compare in terms of baseline scatter. In Table 6 we compare the baseline length repeatabilities using a linear approximation. In Fig. 4 the wrms of the estimated baseline length is plotted for solutions estimated with pSolve (upper figure) and with VieVS (lower figure). In both figures the red crosses denote the baselines determined from the MOJAVE experiments and the blue x-signs depict the VLBA baselines estimated from RDV&CN sessions when the whole scheduled network (i.e., with the non-VLBA telescopes) was adjusted in the analysis. The green diamonds in the upper figure show the wrms for the VLBA baselines from
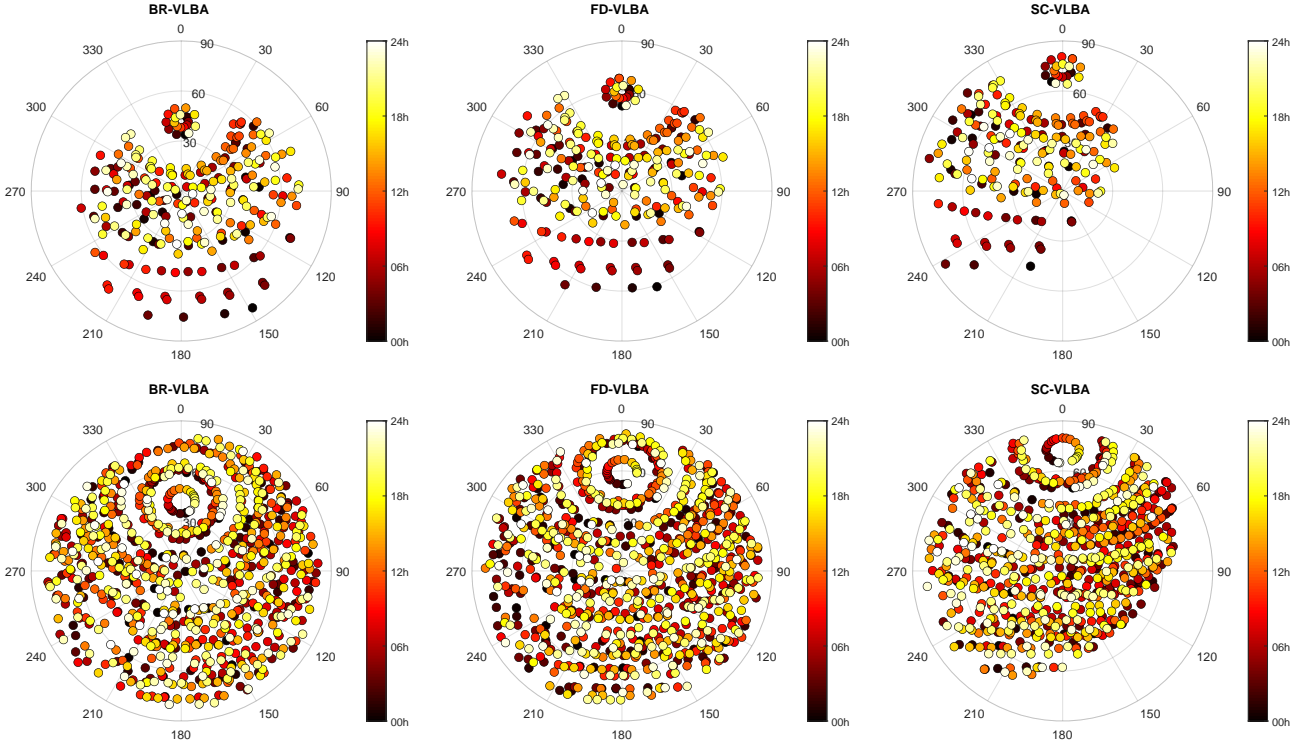
Fig. 2 Sky coverage

Table 5 Mean number of scans at VLBA telescopes in one session computed over the period of interest (September 2016 - July 2020).

	Br	Fd	Hn	Kp	La	Mk	Nl	Ov	Pt	Sc
MOJAVE BL229 series	245	245	241	248	251	204	251	252	235	219
geodetic RDV&CN experiments	451	485	445	493	483	357	467	487	451	423

Table 6 Baseline length scatter. Coefficients of a linear approximation: $a \cdot L + b$ where L is length of baseline in [mm].

	software	a	b
BL229	PIMA, pSolve	$9.12e^{-10}$	2.50
BL229	PIMA, VieVS	$9.79e^{-10}$	2.04
RDV&CN VLBA only	PIMA, pSolve	$6.41e^{-10}$	1.51
RDV&CN all stat	PIMA, pSolve	$6.14e^{-10}$	1.54
RDV&CN all stat	PIMA, VieVS	$8.13e^{-10}$	0.81
RDV&CN all stat	vgosDB, VieVS	$5.98e^{-10}$	1.17

RDV&CN sessions when measurement at non-VLBA stations was removed from the analysis. Brown circles in the lower figure show the baseline scatter at VLBA stations when the vgosDB for the RDV&CN sessions were taken as input in the VieVS software.

– comparable baseline scatter for MOJAVE sessions from pSolve and VieVS
– similar baseline scatter for VLBA telescopes with/witout non-VLBA stations
– lowest baseline scatter from the vgosDB ...

Earth orientation parameters The Earth orientation parameters are estimated in a so-called backward solution, i.e., a solution consistent with globally estimated terrestrial and celestial reference frame from the respective sessions. The orientation of the TRF is set with the NNT/NNR condition on all 10 VLBA stations and the CRF is oriented with the NNR condition on ICRF3 defining sources in VieVS and on selected (??? the listed sources in the .cnt are not the icrf2 defining sources...) sources in pSolve. Several solutions similar to that introduced in the afore-noted paragraph are computed and the EOP estimated in pSolve and VieVS are depicted in Figs. 5 and 6, respectively. Differences between the EOP MOJAVE and RDV&CN series are characterized in Table 7 in terms of the relative offset, relative drift and wrms for each of the five EOP, i.e., the two polar motion components (x-pole, y-pole), the rotation dUT1, and the two nutation offsets (dX, dY). Table 8 contains the median formal error for the respective EOP time series.
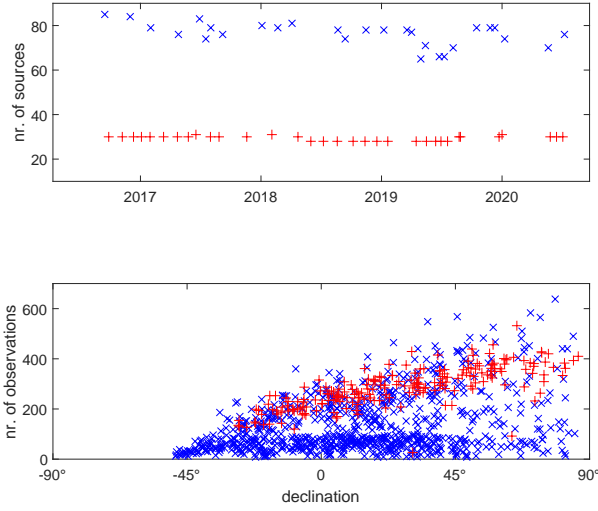
Fig. 3 The upper plot shows number of observed sources in each session. The lower plot depicts the median number of observations for each source. The red crosses stand for the BL229 experiments, blue x-signs for the RDV&CN experiments.

Table 7 EOP statistics of the differences between MOJAVE and RDV&CN series. Difference in wrms is computed w.r.t. the linear trends.

	x-pole	y-pole	dUT1	dX	dY
MOJAVE w.r.t. RDV&CN all stat (PIMA, pSolve)					
offset [μ(a)s]	-10.8	76.6	-11.1	-	-
drift [μ(a)s/y]	46.0	-93.8	3.5	-	-
wrms [μ(a)s]	180.9	191.8	10.1	97.1	40.4
MOJAVE w.r.t. RDV&CN VLBA only (PIMA, pSolve)					
offset [μ(a)s]	-11.2	-13.2	-9.4	-	-
drift [μ(a)s/y]	111.0	-151.4	0.1	-	-
wrms [μ(a)s]	144.1	62.7	7.0	80.3	-1.7
MOJAVE w.r.t. RDV&CN VLBA only (PIMA, VieVS)					
offset [μ(a)s]	-335.8	335.2	7.6	-	-
drift [μ(a)s/y]	119.4	-224.1	0.4	-	-
wrms [μ(a)s]	85.2	49.6	8.8	-1.3	62.1
MOJAVE w.r.t. RDV&CN VLBA only (vgosDB, VieVS)					
offset [μ(a)s]	-327.2	878.0	-2.7	-	-
drift [μ(a)s/y]	-5.9	299.7	-0.9	-	-
wrms [μ(a)s]	69.4	-8.7	1.2	-5.3	67.0

3 Ionosphere

The ionosphere is a refractive media. Propagating in the ionosphere, phase delay decreases, and group delay τ_{gr} increases with respect to the ionosphere free τ_{if} group delay in the absence of the ionosphere

$$\tau_{gr} = \tau_{if} + \kappa \Delta \text{TEC}/f_{\text{eff}}^2$$

where f_{eff} is the effective frequency that is within several pro cents from the recorded central sky frequency,

Δ TEC is the differential total electron contents measured in TECU units (1 TECU = 10^{16} electron/m^2):

$$\Delta \text{TEC} = \int N_v \, ds_1 - \int N_v \, ds_2$$

s_1 and s_2 are paths of wave propagation from a source to the first and second station of the radio interferometer and

$$\kappa = 10^{-16} \cdot \frac{e^2}{2 \, c \, m_e \, \epsilon_o} = 5.308018 \cdot 10^{10} s^{-1}$$

e — charge of an electron, m_e — mass of an electron, ϵ_o — permittivity of free space, c — velocity of light in vacuum.

To mitigate the impact of the ionosphere on group delay, geodetic observations are usually conducted at two frequencies simultaneously. Combining group delays τ_u and τ_l at the upper and lower frequencies f_u and f_l respectively, we can drive the differential TEC and the ionosphere free path delay as

$$\Delta TEC = \frac{f_u^2 f_l^2}{f_u^2 - f_l^2} \, (\tau_l - \tau_u)$$
$$\tau_{if} = \frac{f_u^2}{f_u^2 - f_l^2} \, \tau_u - \frac{f_l^2}{f_u^2 - f_l^2} \, \tau_l$$
$$\tau_{iu} = \frac{f_l^2}{f_u^2 - f_l^2} \, (\tau_l - \tau_u)$$

Derivations of this equations can be found for example in Petrov et al. (2011)

This approach allows effectively cancel the ionospheric contribution, leaving residual contribution at a level not exceeding several ps (Hawarey et al., 2005).

MOJAVE program used only one frequency. An alternative approach for modeling the ionospheric contribution is to use TEC maps from processing GNSS observations. Applying time and spacial interpolation, we can compute TEC in the up direction for each station, each observation. Then we can related the TEC into direction of observation at elevation E to TEC in vertical direction to the via mapping function $M_i(E)$. Considering the ionosphere as a thin shell at height H, we can easily derive the mapping function as

$$\beta(E) = \arcsin \frac{\cos E}{1 + \frac{H}{R_\oplus}}$$
$$M_i(E) = \frac{1}{\cos \beta(E)},$$
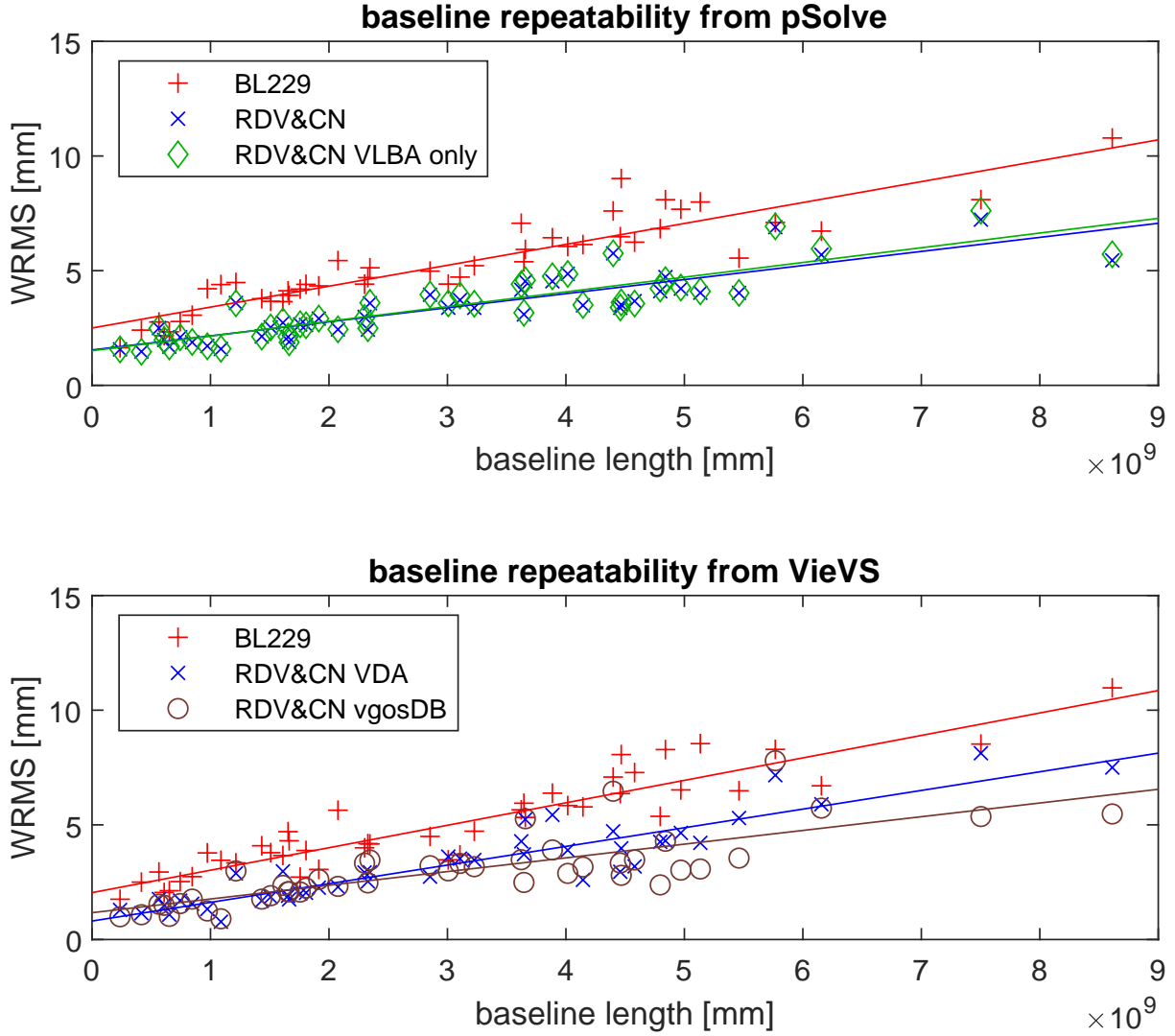
where $R_\oplus$ is the Earth's radius.

baseline repeatability from pSolve

baseline repeatability from VieVS

Fig. 4 Baseline length scatter. Without iono correction.

Table 8 Median formal errors for the EOP estimates from backward solution.

	x-pole [μas]	y-pole [μas]	dUT1 [μs]	dX [μas]	dY [μas]
MOJAVE (PIMA, pSolve)	108.6	153.3	8.6	59.1	56.1
RDV&CN all stat (PIMA, pSolve)	56.9	89.1	3.6	85.6	60.2
RDV&CN VLBA only (PIMA, pSolve)	79.7	119.6	5.7	91.7	69.1
MOJAVE VLBA only (PIMA, VieVS)	81.9	97.4	6.9	50.1	55.4
RDV&CN VLBA only (PIMA, VieVS)	50.9	62.1	4.2	39.0	36.6
RDV&CN VLBA only (vgosDB, VieVS)	72.1	92.2	6.1	76.8	65.6

We used Center for Orbit determination in Europe (CODE) TEC time series (Schaer, 1999)[4] with a resolution of $5° \times 2.5° \times 2^h$. This resolution is relatively coarse and accounts only a part of the signal. Therefore, our

results of processing MOJAVE results are affected by systematic errors caused by the residual ionosphere.

In order to quantify the residual ionospheric signal, we process dual-band RV+CN data set. For the purpose of this study, we consider that the ionospheric free linear combination of X and S and group delays has no ionospheric contribution. We can form the differences

---

[4] Available at ftp://ftp.aiub.unibe.ch/CODE
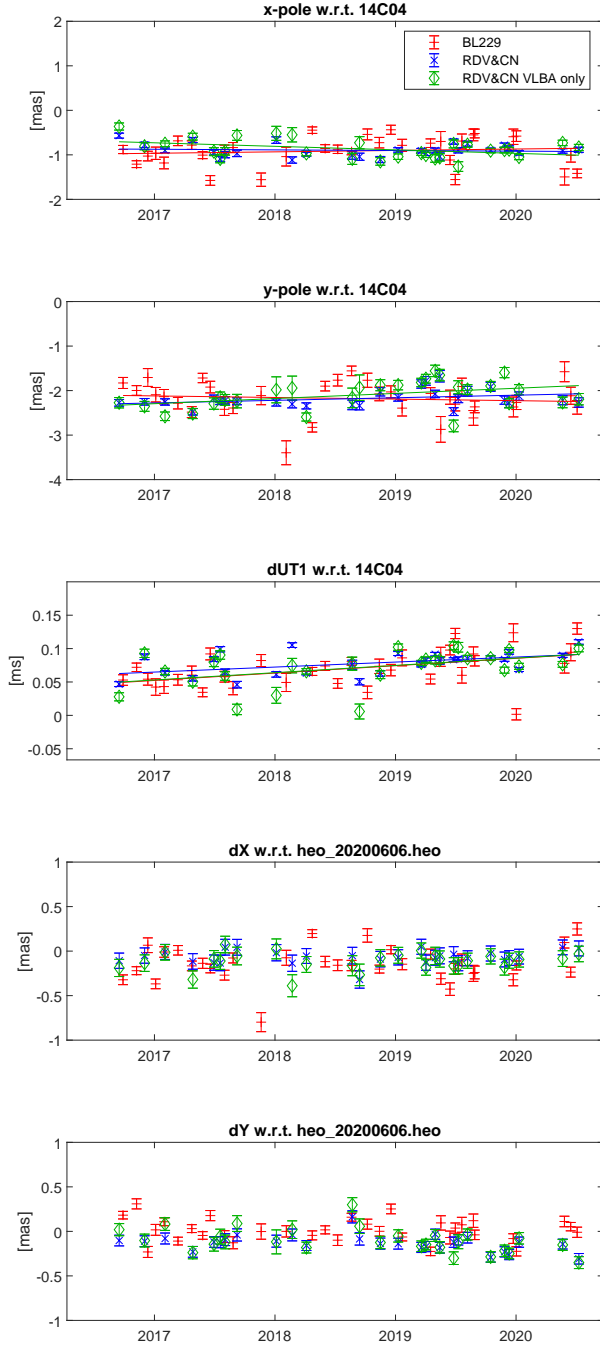
Fig. 5 EOP from pSolve

Fig. 6 EOP from VieVS

between the ionospheric contribution computed TEC maps and from X and S and group delays and investigate the properties of this stochastic process.

Solving for zenith path delay in the neutral atmosphere will pick up a portion of the slowly variating bias, but the ionospheric fluctuations at scales less than several hours will propagate to residuals. We can try to characterize stochastic properties of the residual sig-
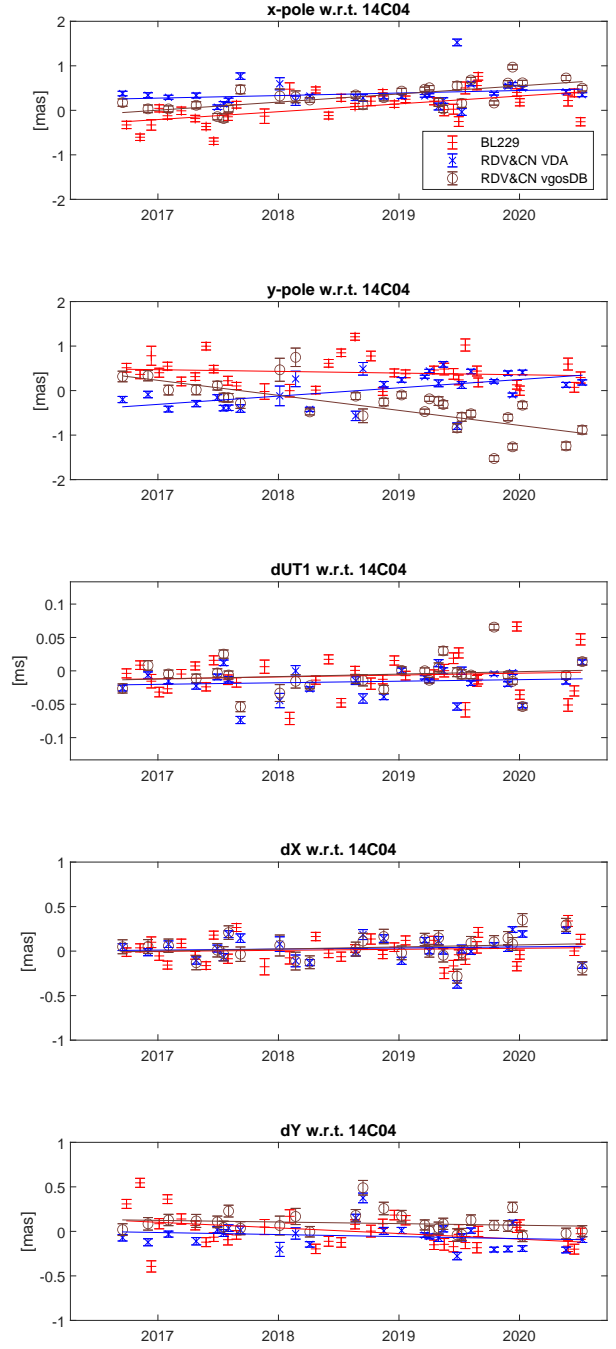
nal. The ionospheric path delay fluctuations is a nonstationary process. From the general results or turbulence theory, We can expect that fluctuations at scales x will be related to fluctuations at scales y via a power law. Therefore, we did the following:

First, we computed the mean differences $d_{gv} = \tau_{ig} - \tau_{iv}$ between the ionospheric path delay at X-band computed from TEC maps (τ_{ig}) and from VLBI dual band
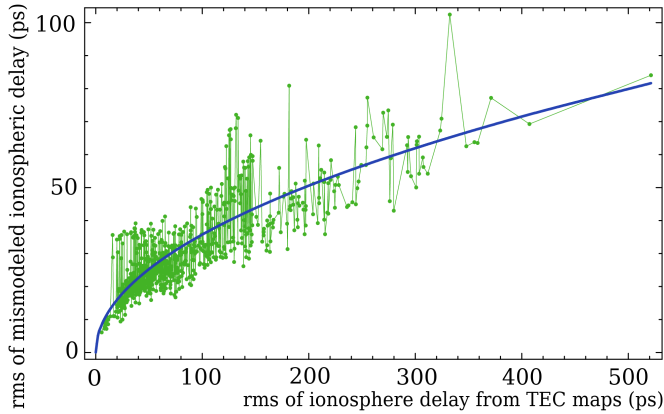
Fig. 7 The relationship between rms of the errors in iono-spheric path delay computed from TEC maps as a function of rms of the variations of group delays derived from TEC maps (green dots). The solid blue line shows a regression in a from of the power law 1/2.

observables (τ_{iv}) every baseline and every experiment in rv+cn dual-band dataset. And then we subtracted that mean value. The mean vale is the sum of the bias between TEC maps and VLBI ionospheric path delay and instrumental delay in VLBI hardware. The instrumental delay may be greater than the ionospheric signal. Since the instrumental delay is not calibrated, the mean d_{gv} is meaningless. Then we computed the rms of over d_{gv}. We discarded the data with clock jumps that may happen at only one band. We got time series of rms(d_{gv}). We examined empirical relationships of rms(d_{gv}) with other statistics. We found that rms^2(d_{gv}) has a linear dependence with rms(τ_{ig}). The power law dependence of (d_{gv}) and τ_{ig} was expected, but the power law coefficient, 2, is purely empirical. Figure 7 demonstrate the time series of d_{gv} and their fit.

We can compute the rms of the ionospheric errors at a given baseline of a given experiment via

$$\mathrm{rms}(d_{gv}) = \sqrt{12.8\,\mathrm{rms}(\tau_{ig})},$$

where the rms is expressed in ps. This empirical relationship allows us to predict the second moment of the residual noise after we perform data reduction for the ionospheric contribution using the TEC maps. One can expect that if the TEC variance is greater, the residual errors are also greater. Expression 3 shows how much greater.

We have computed baseline-dependent additive noise due to mismodeled ionosphere for every baseline and every experiment of MOJAVE program using τ_{ig}. We added that noise to the a priori group delay errors in quadrature and computed new weights. We ran several baseline solutions, computed baseline repeatabilities, and compared them with the reference dual-band solution using RV+CN data. In solution "bx" we used the
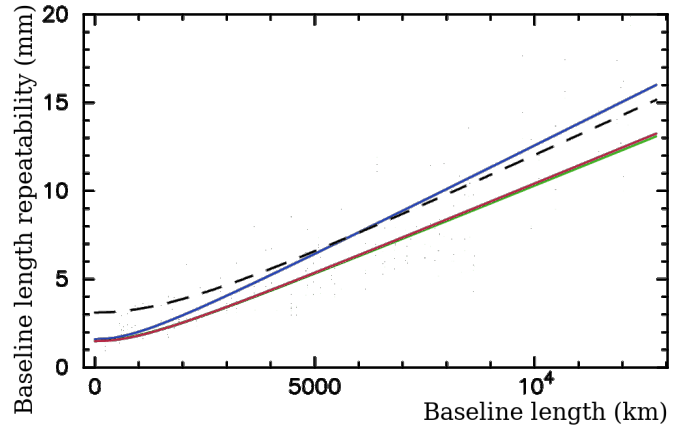

Fig. 8 The dependencies of baseline length repeatability fits on the baseline length. Upper blue curve shows the baseline repeatability for the X-band only "bx" solution that uses GNSS TEC maps. Two lower very close curves, red and green, show the baseline length repeatability for the "bu" solution that shows the effect of mismodeled ionosphere on U-band observable, and the reference dual band solution. The dashed black line shows the baseline length repeatability from the MOJAVE solution.

ionosphere-free computations of group delays, added the contribution of the ionosphere τ_{iu} and processed these data the same way as MOJAVE data, i.e. performed data reduction for the ionosphere using CODE TEC maps and inflating a priori group delay uncertainties for the additional noise due to mismodeling the ionosphere. In the second solution "bu" we simulated how the deficiency of CODE TEC model would alter RV+CN solution, as if these experiments ran at 15.3 GHz instead of 8.6/2.3 GHz. To achieve this, we re-scaled τ_{iu} by the square of the frequency ratio $(8.64/15.28)^2 \approx 0.32$. Figure 8 shows fit in a form $\sqrt{a^2 + (b\,L)^2}$ for all these solutions. The baseline length repeatability from MOJAVE solution is shown by the dashed line.

We found that the impact of the mismodeling ionosphere on the baseline length repeatability of U-band VLBA data collect4ed in 2016–2020 during Solar minimum is negligible. Therefore, an increase in the baseline length repeatability from a geodetic solution using the MOJAVE dataset with respect to the reference dual-band RV+CN solution cannot be explained by the unaccounted contribution of the ionosphere. We should also caution that this result should not be extrapolated to any estimated parameter, such as source position, and should not be extrapolated to epochs of the Solar maximum.

References

Altamimi Z, Rebischung P, Métivier L, Collilieux X (2016) Itrf2014: A new release of the international terrestrial reference frame modeling nonlinear station motions. Journal of Geophysical Research: Solid Earth 121(8):6109–6131, DOI 10.1002/2016JB013098

Böhm J, Böhm S, Boisits J, Girdiuk A, Gruber J, Hellerschmied A, Krásná H, Landskron D, Madzak M, Mayer D, McCallum J, McCallum L, Schartner M, Teke K (2018) Vienna VLBI and Satellite Software (VieVS) for Geodesy and Astrometry. Publications of the Astronomical Society of the Pacific 130(986):044503, DOI 10.1088/1538-3873/aaa22b

Capitaine N, Wallace P, Chapront J (2003) Expressions for IAU 2000 precession quantities. Astron Astrophys 412(2):567–586, DOI 10.1051/0004-6361:20031539

Charlot P, Jacobs CS, Gordon D, Lambert S, de Witt A, Böhm J, Fey AL, Heinkelmann R, Skurikhina E, Titov O, Arias EF, Bolotin S, Bourda G, Ma C, Malkin Z, Nothnagel A, Mayer D, MacMillan DS, Nilsson T, Gaume R (2020) The third realization of the international celestial reference frame by very long baseline interferometry. A&A 644:A159, DOI 10.1051/0004-6361/202038368

Hawarey M, Hobiger T, Schuh H (2005) Effects of the 2nd order ionospheric terms on VLBI measurements. Geophys Res Lett 32:L11304, DOI 10.1029/2005GL022729

Krásná H, Gordon D, de Witt A, Jacobs CS, Soja B (2019) Earth Orientation Parameters Estimated From K-band VLBA Measurements. In: Haas R, Garcia-Espada S, Lopez Fernandez J (eds) Proceedings of the 24th European VLBI Group for Geodesy and Astrometry Working Meeting, Chalmers University of Technology, vol 24, pp 238–242, DOI 10.7419/162.08.2019, iSBN:978-84-416-5634-5

Lister ML, Aller MF, Aller HD, Hodge MA, Homan DC, Kovalev YY, Pushkarev AB, Savolainen T (2018) MOJAVE. XV. VLBA 15 GHz Total Intensity and Polarization Maps of 437 Parsec-scale AGN Jets from 1996 to 2017. ApJS 234(1):12, DOI 10.3847/1538-4365/aa9c44

Mathews P, Herring T, Buffet B (2002) Modeling of nutation and precession: New nutation series for nonrigid Earth, and insights into the Earth's interior. J Geophys Res 107/B4(2068):26, DOI 10.1029/2001JB000390

Petrov L, Kovalev YY, Fomalont EB, Gordon D (2011) The Very Long Baseline Array Galactic Plane Survey–VGaPS. The Astronomical Journal 142(2):35, DOI 10.1088/0004-6256/142/2/35

Schaer S (1999) Mapping and predicting the Earth's ionosphere using the Global Positioning System. Geod-Geophys Arb Schweiz, Vol 59, 59, http://ftp.aiub.unibe.ch/papers/ionodiss.ps